南京航空航天大学

论文集

（二〇〇八年） 第5册

航空宇航学院

（第5分册）

南京航空航天大学科技部编

二〇〇九年五月

航空宇航学院

第五分册

航空宇航学院2008年学术论文清单（0134）

序号	姓名	职称	单位	论文题目	刊物、会议名称	年、卷、期
1	裘进浩 季宏丽 Matsuta，K 沈星	教授 博士 副教授	0134 0134 0134 0134	Active Noise Isolation of a Plate Structure Without Using Acoustic Sensors	Journal of Intelligent Material Systems and Structures	2008.19.07
2	裘进浩 季宏丽 刘建 朱孔军	教授 博士 博士 副教授	0134 0134 0134 0134	压电功能器件及其在智能结构中的应用	第三届全国压电与声波理论及器件技术研讨会论文集	
3	裘进浩 朱孔军	教授 副教授	0134 0134	Fabrication and performance of functionally graded piezoelectric bending actuators	World Forum on Smart Materials and Smart Structures Technology	
4	Adrien Badel 裘进浩	博士后 教授	0134 0134	A new simple asymmetric hysteresis operator and its application to inverse control of piezoelectric actuators	IEEE TRANSACTIONS ON ULTRASONICS FERROELECTRICS AND FREQUENCY CONTROL	2008.55.05
5	Adrien Badel 裘进浩	博士后 教授	0134 0134	External force and displacement estimation for self-sensing control of a piezoelectric actuator	World Forum on Smart Materials and Smart Structures Technology	
6	Adrien Badel 裘进浩	博士后 教授	0134 0134	Self-Sensing Force Control of a Piezoelectric Actuator	IEEE TRANSACTIONS ON ULTRASONICS FERROELECTRICS AND FREQUENCY CONTROL	2008.55.12
7	Adrien Badel 裘进浩	博士后 教授	0134 0134	Self-sensing high speed controller for piezoelectric actuator	Journal of Intelligent Material Systems and Structures	2008.19.03
8	边义祥 裘进浩 王鑫伟	博士 教授 教授	0134 0134 0132	Constitutive equations of metal-core piezoelectric fibers	南航学报（原文版）	2008.25.03
9	边义祥 裘进浩 王鑫伟 季宏丽 朱孔军	博士 教授 教授 博士 副教授	0134 0134 0132 0134 0134	Actuator of half coated metal core piezoelectric fiber	International Joint Conference of SMSAE/SMEBA 会议上交流	
10	边义祥 裘进浩 王鑫伟 季宏丽 朱孔军	博士 教授 教授 博士 副教授	0134 0134 0132 0134 0134	含金属芯压电纤维振动传感器	第三届全国压电和声波理论及器件技术研讨会 会议上交流	
11	边义祥 裘进浩 王鑫伟 赵永春	博士 教授 教授 硕士	0134 0134 0132 0132	含金属芯压电陶瓷纤维的传感特性研究	压电与声光	2008.30.06
12	陈远晟 裘进浩 朱孔军 季宏丽 边义祥	博士 教授 副教授 博士生 博士生	0134 0134 0134 0134 0134	NEURAL NETWORK BASED INVERSE CONTROL OF PIEZOCERAMIC ACTUATOR	The Third International Conference on Smart Materials & Structures in Aerospace Engineering (3rd SMSAE) The Fourth International Conference on Smart Materials for Engineering & Biomedical Application (4th SMEBA)	
13	顾娜 裘进浩 朱孔军	硕士 教授 教授	0134 0134 0134	A Design of a Flexible Flap System for an Adaptive Wing	International Joint Conference of SMSAE/SMEBA 2008	
14	季宏丽 Adrien Badel 裘进浩 Elie Lefeuvre	博士生 教授 教授	0134 外单位 0134	Piezoelectric vibration damping by an enhanced semi-passive method	12th Asia-Pacific Vibration Conference	

15	季宏丽 马勇 裘进浩 姜皓 沈辉 朱孔军	博士 硕士 教授 硕士 硕士 副教授	0134 0134 0134 0134 0134 0134	Optimal design of high efficiency piezoelectric energy harvester	光学精密工程	2008.16.12
16	季宏丽 裘进浩 Adrien Badel 朱孔军	博士 教授 副教授	0134 0134 0134	SEMI-ACTIVE VIBRATION CONTROL OF A COMPOSITE BEAM USING AN ADAPTIVE SSDV APPROACH	Proceeding of SMSAE/SMEBA2008	
17	季宏丽 裘进浩 陈远晟 朱孔军	博士 教授 博士生 副教授	0134 0134 0134 0134	Multimodal vibration control using a synchronized switch based on a displacement switching threshold	the Fifth International Conference on Flow Dynamics	
18	季宏丽 裘进浩 赵永春 朱孔军	博士 教授 硕士 副教授	0134 0134 0132 0134	基于压电元件的半主动振动控制的研究	振动工程学报	2008.21.0
19	季宏丽 裘进浩 朱孔军	博士 教授 副教授	0134 0134 0134	VIBRATION CONTROL OF A COMPOSITE BEAM BY AN ADAPTIVE SEMI-ACTIVE METHOD BASED ON LMS ALGORITHM	第三届全国压电与声波理论及器件技术研讨会论文集	
20	李勇君 裘进浩 朱孔军 季宏丽	硕士 副教授 教授 博士	0134 0134 0134 0134	PNN-PZT 陶瓷流延浆料流变性能研究	电子元件与材料	2008.27.12
21	刘建 裘进浩 常伟杰 边义祥 朱孔军	博士 教授 硕士 博士 副教授	0134 0134 0134 0134 0134	含金属芯压电纤维对Lamb波的传感响应研究	第三届全国压电与声波理论及器件技术研讨会论文集	
22	沈辉 季宏丽 裘进浩 Adrien Badel 马勇 姜皓	博士 博士 教授 硕士 硕士	0134 0134 0134 0134 0134	Self-powered vibration damping system by a semi-passive technique	the Fifth International Conference on Flow Dynamics	
23	沈辉 裘进浩 Marco Balsi Francesco dell' Isola Ivan Giorgio	博士 教授	0134 0134	Self-powered vibration damping system by a semi-passive technique	International Joint Conference of SMSAE/SMEBA 2008	
24	王道利 裘进浩 朱孔军 季宏丽 谢实辉	硕士 教授 副教授 博士 硕士	0134 0134 0134 0134 0134	EFFECTS OF DIFFERENT Sb ADDITION ON [(K0.44Na0.52) Li0.04](Nb0.9-xTa0.1Sbx)O3 LEAD-FREE PIEZOCERAMICS	Proceedings of the 2008 symposium on piezoelectricity, acoustic waves and device applications	2008.12
25	翟太珍 裘进浩 陈远晟	硕士 教授 博士	0134 0134 0134	Design of Feedback Control System for Vibration Exciter Based on ATmega16	The Third International Conference on Smart Materials & Structures in Aerospace Engineering	
26	袁慎芳 梁大开 石立华 赵霞 吴键 李刚 邱雷	教授 教授 教授 博士 博士 博士 博士	0134 0134 0134 0134 0134 0134 0134	Recent Progress on Distributed Structural Health Monitoring Research at NUAA	Intelligent Material Systems and Structures	2008.19.03
27	丁建伟 袁慎芳 吴键 李耀曾	硕士 教授 博士 硕士	0134 0134 0134 0134	Design and Evaluation of a Wireless Sensor Network Based Structural Strain Monitoring System	International Joint Conference of SMSAE/SMEBA 2008	
28	李刚 石立华 袁慎芳 王鑫伟	博士 教授 教授 教授	0134 0134 0134 0134	基于预置压电阵列的Lamb波检测技术研究	压电与声光	2008.30.03

29	李耀曾 袁慎芳 吴键 丁建伟	硕士 教授 博士 硕士	0134 0134 0134 0134	Design of a Wireless Sensor Node with High-speed Sampling Rate	International Joint Conference of SMSAE/SMEBA 2008	
30	宁宁 袁慎芳 沈真 张积广	硕士 教授 研究员 研究员	0134 0134 0134 0134	在役航空复合材料结构的无损检测技术	航空制造技术	2008. 15
31	邱雷 袁慎芳	博士 教授	0134 0134	A Low Crosstalk Switch Unit for Dense Piezoelectric Sensor Networks	International Joint Conference of SMSAE/SMEBA 2008	
32	邱雷 袁慎芳	博士 教授	0134 0134	集成压电健康监测扫查系统的研制及其应用	压电与声光	2008. 30. 01
33	邱雷 袁慎芳 王强	博士 教授 博士	0134 0134 0134	基于Lamb波主动结构健康监测系统的研制	交通部大跨径桥梁结构损伤预警及状态评估技术研讨会	
34	邱雷 袁慎芳 王强 蔡建 周恒保 张炳良	博士 教授 博士 博士 硕士 硕士	0134 0134 0134 0134 0134 0134	压电多通道扫查结构健康监测系统的研制	测控技术	2008. 27. 增刊
35	尚 盈 袁慎芳 吴 键 丁建伟 李耀曾	硕士 教授 博士 硕士 硕士	0134 0134 0134 0134 0134	用于应变监测的无线传感器网络节点的设计	传感器与微系统	2008. 27. 07
36	孙亚杰 袁慎芳 蔡建	博士 教授 博士	0134 0134 0134	基于超声相控阵的材料结构健康监测实验研究	宇航学报	2008. 29. 04
37	孙亚杰 袁慎芳 邱雷 王强	博士 教授 博士 博士	0134 0134 0134 0134	基于Lamb波和相控阵的复合材料损伤识别研究	测控技术	2008. 27. 增刊
38	王长坤 袁慎芳 邱雷 黄红梅	硕士 教授 博士 博士	0134 0134 0134 0134	基于支持向量机的加筋板健康监测	传感器与微系统	2008. 27. 05
39	王强 袁慎芳	博士 教授	0134 0134	航空结构健康监测的压电夹层设计	传感器与微系统	2008. 27. 07
40	王强 袁慎芳	博士 教授	0134 0134	主动Lamb波结构健康监测中信号增强与损伤成像方法	宇航学报	2008. 29. 04
41	王强 袁慎芳 邱雷 孙亚杰	博士 教授 博士 博士	0134 0134 0134 0134	基于时间反转理论的结构损伤图像表征方法	仪器仪表学报	2008. 29. 09
42	王强 袁慎芳 邱雷 孙亚杰	博士 教授 博士 博士	0134 0134 0134 0134	基于时间反转理论及压电阵列技术的损伤图像监测方法	测控技术	2008. 27. 02
43	吴键 袁慎芳 王子龙 丁建伟 李耀曾	博士 教授 本科 硕士 硕士	0134 0134 0134 0134 0134	面向结构监测的无线传感网络应用研究	交通部大跨径桥梁结构损伤预警及状态评估技术研讨会	
44	吴键 袁慎芳 殷悦 尚盈 丁建伟	博士 教授 硕士 硕士 硕士	0134 0134 0134 0134 0134	基于ZigBee技术的无线传感器网络及其应用研究	测控技术	2008. 27. 01
45	张逍越 袁慎芳 郝桐	博士 教授 本科	0134 0134 0134	Lamb Wave Propagation Modeling for Structure Health Monitoring	International Joint Conference of SMSAE/SMEBA 2008	
46	赵霞 袁慎芳 余振华 叶伟松 曹俊	博士 教授 硕士 硕士 硕士	0134 0134 0134 0134 0134	Designing strategy for multi-agent system based large structural health monitoring	Expert Systems With Applications	2008. 34. 02

47	赵霞 袁慎芳 周恒保 孙红兵	博士 教授 硕士 博士	0134 0134 0134 0134	基于声发射技术的损伤诊断Agent研究	中国机械工程	2008. 19. 014
48	赵霞 袁慎芳 周恒保 孙红兵	博士 教授 硕士 博士	0134 0134 0134 0134	基于主体协作的盒段级结构健康监测系统	压电与声光	2008. 30. 05
49	曹俊 袁慎芳 蔡建 邱雷 余振华	硕士 教授 博士 博士 硕士	0134 0134 0134 0134 0134	疲劳裂纹扩展的实时健康监测	压电与声光	2008. 30. 06
50	徐欣 袁慎芳	硕士 教授	0134 0134	基于Lamb波的主动监测系统温度效应研究	传感器世界	2008. 2
51	徐欣 袁慎芳	硕士 教授	0134 0134	结构载荷定位系统的温度补偿研究	压电与声光	2008. 30. 03
52	周恒保 袁慎芳 赵 霞 孙红兵	硕士 教授 博士 博士	0134 0134 0134 0134	基于主动监测的大型结构连接失效的远程监测	传感器与微系统	2008. 27. 07
53	李季平 梁大开	博士 教授	0134 0134	基于计算机图像法测量物体位移及应变	激光杂志	2008. 29. 04
54	李秋锋 石立华 梁大开	博士 教授	0134 0134 0134	基于合成孔经聚焦技术的混凝土断面二维成象的方法研究	声学学报	2008. 33. 07
55	李秋锋 石立华 邬冠华 梁大开	博士 教授	0134 0134 0134 0134	提高混凝土结构成像质量的技术研究	仪器仪表学报	2008. 29. 11
56	李秋锋 石利华 梁大开	博士 教授	0134 0134	混凝土检测中基于数字滤波器的传感器补偿方法	南京航空航天大学学报	2008. 40. 01
57	陆观 梁大开	博士 教授	0134 0134	基于粒度计算的光纤智能结构监测	传感器与微系统	2008. 27. 06
58	王彦 梁大开	博士 教授	0134 0134	基于长周期光纤光栅微弯特性的智能结构振动监测	仪器仪表学报	2008. 29. 06
59	王彦 梁大开	博士 教授	0134 0134	基于光栅光谱分析的混凝土结构刚劲锈蚀监测	光谱学与光谱分析	2008. 28. 11
60	王彦 梁大开	博士 教授	0134 0134	强度解调的光纤光栅智能结构动态监测技术	光电子、激光	2008. 19. 03
61	张伟 梁大开	硕士 教授	0134 0134	光纤光栅传感器系统信号介调技术的研究	压电与声光	2008. 30. 06
62	周兵 梁大开	硕士 教授	0134 0134	长周期光纤光栅的一种温度补偿方法	压电与声光	2008. 30. 02
63	徐志伟 黄雪峰 沈星	副教授 硕士 副教授	0134 0134 0134	基于PT和MFC的飞机垂直尾翼振动主动控制	南京航空航天大学学报	2008. 40. 03
64	王海风 徐志伟	硕士 副教授	0134 0134	结构吸波材料电磁散射特性的数值仿真	机械科学与技术	2008. 27. 11
65	王海荣 徐志伟	硕士 副教授	0134 0134	用于振动主动控制的DSP系统设计与实现	微计算机信息	2008. 24. 10-1
66	吴志华 徐志伟	硕士 副教授	0134 0134	时域辨识在垂尾智能结构控制系统中的应用	振动、测试与诊断	2008. 28. 01
67	邓力元 陈仁文 侯志伟	硕士 教授 博士	0134 0134 0134	SOGFCMAC Fuzzy artificial neural network for active vibration control of flexible plate	World Forum on Smart Materials and Smart Structures Technology	
68	韩芳芳 陈仁文 刘强	硕士 教授 博士	0134 0134 0134	Optimal design method for sensors/actuators placement in the active vibration control of a 2D flexible plate	World Forum on Smart Materials and Smart Structures Technology	
69	侯志伟 陈仁文 孟元元	博士 教授 硕士	0134 0134 0134	A new temperature compensation method for flow measurement employing FLNN	World Forum on Smart Materials and Smart Structures Technology	
70	刘强 陈仁文 顾宝成	博士 教授 硕士	0134 0134 0134	Research on signal separation of self-sensing piezoelectric actuator	World Forum on Smart Materials and Smart Structures Technology	
71	田 旭 陈仁文	硕士 教授	0134 0134	Design of intelligent flow auto-monitoring system-based on GPRS wireless network	World Forum on Smart Materials and Smart Structures Technology	

72	郑世杰	教授	134	A novel FE model for the active control of FGM plates with integrated piezoelectric sensors and actuators	1st International Conference on Computational Methods	2006.01
73	郑世杰 冯岩 代锋	教授 硕士生 硕士生	0134 0134 0134	The simulation of active control of the shape and vibration of piezoelectric, Magneto-electro-elastic and FGM structures	Proceedings of the 2008 symposium on piezoelectricity, acoustic waves and device applications.	2008
74	董会丽 郑世杰	硕士生 教授	0134 0134	有限元分析与RBF神经网络结合的荷载识别	工程力学	2008.25.03
75	李正强 郑世杰	硕士生 教授	0134 0134	基于HHGA—RBF神经网络的复合材料结构脱层损伤监测研究	中国宇航学报	2008.29.01
76	张荣祥 郑世杰 夏庆观	硕士生 教授 副教授	0134 0134 0134	基于Hilbert 扫描和小波变换的自适应图像分割	中国图象图形学报	2008.13.04
77	张荣祥 郑世杰 夏彦君	硕士生 教授 硕士生	0134 0134 0134	Strain profile reconstruction of fiber Bragg grating with gradients using chaos genetic algorithm and modified transfer matrix formulation	Optics Communications	2008.281.13
78	张荣祥 郑世杰 夏彦君	硕士生 教授 硕士生	0134 0134 0134	支持向量回归算法在光纤光栅非均匀应变重构中的应用	光学学报	2008.28.08
79	沈星	副教授	0134	Study of Rainbow Actuator and its Intergation with SMA	Jounal of Intelligent Material Systems and Structures	2008.19
80	沈星 王鑫伟	副教授 教授	0134 0132	发挥高校实验室的科研优势提高本科生毕设教学质量	南京航空航天大学学报（社会科学版）	2008.10.01
81	李允 沈星	硕士 副教授	0134 0134	基于ANSYS的1-3型压电纤维复合材料结构优化	航天制造技术	2008.04
82	李允 沈星 王宁	硕士 副教授 硕士	0134 0134 0134	1-3型压电纤维复合材料结构参数对驱动性能的影响	材料导报	2008.22.12
83	李允 沈星 王宁	硕士 副教授 硕士	0134 0134 0134	压电陶瓷驱动器性能的理论计算与ANSYS仿真	安徽工业大学学报	2008.25.04
84	刘永刚 沈星	博士 副教授	0134 0134	交叉指型电极压电振子的谐 振特性研究	压电与声光	2008.30.03
85	朱孔军 裘进浩	副教授 教授	0134 0134	HAp/TCP Composites Prepared by Hydrothermal Hot-Pressing Technique	Proceeding of ICAMS-2	2008
86	朱孔军 裘进浩	副教授 教授	0134 0134	Hydrothermal Synthesis and Crystallographic study of Sr-Pb Hydroxyapatite Solid Solutions	Journal of the Ceramics Society of Japan	2007.115
87	朱孔军 裘进浩	副教授 教授	0134 0134	Hydrothermal Synthesis of KxNa1-xNbO3 Powders for Fabrication of Lead-free Piezoelectric Ceramics	World Forum on Smart Materials and Smart Structures Technology	2008
88	朱孔军 裘进浩	副教授 教授	0134 0134	Hydrothermal Synthesis of $Na(Nb_{1-x}Ta_x)O_3$ Powder for Fabrication of Lead-Free Piezoelectric Ceramics	Key Engineering Materials	2008.368-372
89	朱孔军 苏礼奎 季宏丽 裘进浩	副教授 教授	0134 0134	New Method for Fabrication of Lead-Free BaTiO3 Piezoelectric Ceramics	Proceedings of The 2008 Symposium on Piezoelectricity, Acoustic Waves and Device Application	2008
90	陈延东 朱孔军 季宏丽 裘进浩 李勇军	硕士 副教授 博士 教授 硕士	0134 0134 0134 0134 0134	弛豫型PNN-PZT压电陶瓷的制备与性能研究	中国科协第185次青年科学家论坛	
91	李勇君 朱孔军 裘进浩 季宏丽	硕士 副教授 教授 博士	0134 0134 0134 0134	PNN-PZT功能梯度压电弯曲驱动器的制备	中国科协第185次青年科学家论坛	

92	谢实辉 朱孔军 裘进浩 郭华	硕士 副教授 教授 硕士	0134 0134 0134 0134	Microstructure and electrical properties of NaNbO3-BaTiO3 lead-free piezoelectric ceramics	Joint conference of the third international conference on Smart Materials & Structures in Aerospace Engineering/the fourth international Conference on Smart Materials for Engineering & Bimedical Applications (SMSAE/SMEBA 2008)	2008-7-1论文编号：0426
93	潘晓文 曾捷 梁大开	博士 讲师 教授	0134 0134 0134	基于光纤智能夹层的损伤检测系统	压电与声光	2008.30.06
94	葛瑞钧 王帮峰 牟常伟 周勇	硕士 教授 硕士 博士	0134 0134 0134 0134	Research on deformation characteristics of corrugated composites for morphing wing	SMSAE/SMEBA 2008	
95	金宁 王帮峰 卞侃 陈骐 熊克	硕士 教授 博士 硕士 教授	0134 0134 0134 0134 0134	Comparative Study on the Performance of IPMC by Different Surface Roughen Methods	SMSAE/SMEBA 2008	
96	金宁 王帮峰 卞侃 陈骐 熊克	硕士 教授 博士 硕士 教授	0134 0134 0134 0134 0134	表面粗化工艺对IPMC的制备及性能的影响	功能材料	2008.39.11
97	钱黄生 王帮峰 周勇 荀磊	硕士 教授 博士 硕士	0134 0134 0134 0134	Numerical analysis on the cymbal and half cymbal membranes for piezoelectric synthetic jet actuator	SMSST07	
98	王帮峰 陈仁文	教授 教授	0134 0134	Leakage Location system for oil pipeline on basis of stress wave detection	Frontiers of Mechanical Engineering in China	2008.03.03
99	王帮峰 秦霞	教授 硕士	0134 0134	Numerical Analysis on Two Kinds of Cymbal Membranes for Piezoelectric Micro-Flow Actuator	Jouranl of Intelligent Material Systems and Structures	2008.18.03
100	荀磊 王帮峰 钱黄生	硕士 教授 硕士	0134 0134 0134	Research on the variable voltage frequency inverter-based on DSP for piezoelectric micro-jet actuator	SMSST07	
101	周勇 王帮峰	博士 教授	0134 0134	Research on Fluidic Dynamic Characteristic of the Piezoelectric Synthetic Jet Actuator	Jouranl of Intelligent Material Systems and Structures	2008.18.03
102	周勇 王帮峰 张立 钱黄生 王鑫伟	硕士 教授 博士 硕士 教授	0134 0134 0134 0134 0134	Research on the structures and geometric parameters of synthetic jet actuator	SMSST07	
103	安逸 熊克 王帮峰 顾娜	博士 教授 教授 硕士	0134 0134 0134 0134	A Continuum Electromechanical Model of IPMC Based on Irreversible Thermodynamics Theory High Voltage Pulse	SMSAE/SMEBA 2008	
104	陈骐 熊克 卞侃 金宁 王帮峰	硕士 教授 博士 硕士 教授	0134 0134 0134 0134 0134	Study on the Preparation and Performance of Ion-exchange Polymer Metal Composites (IPMC) Based on Silver Electrode	SMSAE/SMEBA 2008	
105	沈辉 于敏 季宏丽 戴振东 裘进浩	博士 博士 教授 教授	0134 0134 0134 0134	IPMC的力输出特性	功能材料	2007.38.09
106	姜皓 裘进浩 朱孔军	硕士 教授 副教授	0134 0134 0134	压电陶瓷驱动器的迭代学习逆补偿混合控制	江苏航空	2008.增刊
107	沈辉 于敏 季宏丽 戴振东 裘进浩	博士 博士 教授 教授	0134 0134 0134 0134	IPMC的力输出特性	功能材料	2007.38.09

World Forum on Smart Materials and Smart Structures Technology – Spencer Jr (ed)
 ISBN 978-0-415-46845-9

Research of smart materials and structures at NUAA

Jinhao Qiu

Aeronautical Key Laboratory for Smart Materials & Structures, College of Aerospace Engineering, Nanjing University of Aeronautics & Astronautics, Nanjing, China

ABSTRACT: The research activities of the Aeronautic Science Key Lab for Smart Materials and Structures, Nanjing University of Aeronautics and Astronautics are introduced. The research fields include structural health monitoring, structural vibration reduction and noise suppression, adaptive wing and smart rotor, sensor and actuation technology, functional materials and devices, and system integration and measurement technology. Three fields of research are introduced in detail. The first field is the structural health monitoring (SHM). Research subjects includes hybrid structural health monitoring using FBG sensors and piezoelectric sensors, wireless sensor network, multi-agent based distributed SHM technology, and braided composites with embedded optic fibers. The second field introduced is development of high-performance piezoelectric materials using a novel sintering process consisting of microwave heating and hot-press. This approach is applied to the fabrication of PZT and PNN-PZT materials and their properties were improved significantly. The third field introduced is the development of high-performance piezoelectric devices, including functionally graded piezoelectric actuators and piezoelectric fibers. The functionally graded piezoelectric actuators are fabricated by gradually changing the piezoelectric and dielectric properties of the materials in the thickness direction of the actuator.

1 INTRODUCTION

The Aeronautical Science Key Laboratory for Smart Materials & Structures at Nanjing University of Aeronautics and Astronautics (NUAA) is the only ministerial-level key laboratory in China at present, which is specialized in smart materials and structures. In 1991, a multidisciplinary research team was organized at NUAA to carry out research in the new field of smart materials and structures. With the development of the team, a key laboratory was established by the former Aviation Industry Corporation of China (AVIC) in 1997 to further promote research in this important field. After ten years of development, the Lab has further extended its research fields, which include structural health monitoring, structural vibration reduction and noise suppression, adaptive wing and smart rotor, sensor and actuation technology, functional materials and devices, and system integration and measurement technology. Important resources and advanced experimental facilities in the Key Lab include testing system for optical fibers, damage detection systems such as C-scan and acoustic emission systems for composite materials, MTS tension-compression testing machine, structural dynamic analysis system (LMS), data acquisition system, ferroelectric tester (TF-2000), testing system for adaptive wing models, and testing system for smart rotors, etc.

At present, the Laboratory has 7 professors, 3 associate professors, 1 engineer, about 30 Ph.D. students and more than 80 master students. The Lab has more than 2500 m² of space and has received 8 million RMB fund for purchase of new experimental equipment and apparatus for the 5-year period from 2006 to 2010. The average yearly research fund from the government and industry is more than two million RMB.

The researchers in the key lab have undertaken more than 30 important projects in recent years, including two key projects funded by the National Natural Science Foundation. They have also received one national invention award, one national excellent teaching award and twelve provincial and ministerial awards for their innovative and excellent research. Over four hundreds technical papers have been published. Academic relationships have been established with corresponding labs in China, USA, Germany, Japan, France and India for exchanges and collaborations.

In the next three chapters, three research fields of the laboratory are introduced. The first field is the structural health monitoring (SHM). Research subjects includes hybrid structural health monitoring using FBG sensors and piezoelectric sensors, wireless sensor network, multi-agent based distributed SHM technology, and braided composites with embedded optic fibers. The second field introduced is development of high-performance piezoelectric

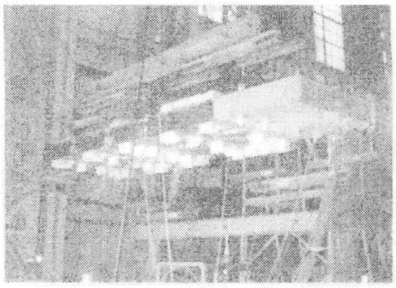

(a) Wing box in bending test

(b) Distributions of sensors in a wing box

Figure 1   Health monitoring of a wing box.

materials using a hybrid sintering process consisting of microwave heating and hot-press. This approach is applied to the fabrication of PZT and PNN-PZT materials and their properties were improved significantly. The third field introduced is the development of high-performance functionally graded piezoelectric actuators. The functionally graded piezoelectric actuators are fabricated by gradually changing the piezoelectric and dielectric properties of the materials in the thickness direction of the actuator.

2   STRUCTURAL HEALTH MONITORING

2.1   *Health monitoring of a Wing box*

A hybrid wing box health monitoring system as shown in Fig. 1(a) was developed based on hybrid piezoelectric sensor array and Bragg grating sensor array [1, 2]. Wing box is an important part of the aircraft structure. The wing box is made of carbon fiber composite material. The PZT sensors and the optic fiber sensors are arranged on the skin. To make it easy to arrange the sensor array and ensure the arrangement process of each element to be the same, the smart layers are manufactured.

The arrangement of the sensor array distribution is shown in Fig. 1(b). A PZT-Fiber integration health monitoring system is developed. Piezoelectric sensor array based active lamb wave diagnostic method and Bragg grating based structural strain monitoring method are realized. Adopting the hybrid monitoring system, the strain field and the temperature field are monitored. The strain distribution was obtained when the wing box is under torsion and bending load. Adopting the hybrid monitoring system, based on PZT sensor array and active wave technique, combined with advanced signal processing method such as time reversal, damage diagnosis is realized. Based of the PZT sensor network, to realize multiple test channels for lamb wave monitoring, any of the PZT sensors can be assigned to act as the actuator or receiver by the computer to excite or sense the lamb wave signal. The damage monitoring process is controlled by an integrated sensor array scanning and damage diagnostic system including hardware and diagnostic software.

2.2   *Wireless sensor network for SHM*

Though the wing box demonstration research is successful, some problems are presented. The key problem is for the big structure, the number of sensors is big and sensor information is tremendous. It is a great challenge for the central computer to sample and process all these data in an acceptable speed. Another problem is when density sensors are adopted, the wires to connect them increase, causing the weight of the whole monitoring system increasing greatly. This is not allowable in lots of application areas, especially in the aircraft. Hence to reduce the weight of the sensor networks, to coordinate and manage the density sensor networks, to fuse the information from different kinds of sensors to take advantage of different estimation methods to make a reliable estimation of the whole structure in an acceptable speed is still a challenge. The distributed structural health monitoring technology for large-scale engineering structures based on smart sensor and multi-agent technology is discussed.

By adopting wireless smart sensor with embedded microprocessors, portion of signal processing and computation can be done locally and simultaneously [3]. The amount of information needs to be transmitted over the network will be reduced greatly and the system speed will be improved. Besides, if the smart sensor adopts the wireless communication links, information can be communicated in a wireless way, which will reduce the weight of the sensor network, thus facilitate densely distributed sensing. Our research is to develop wireless sensor node suitable for SHM requirements: small size, low power, integrated for SHM. Fig. 2 shows the wireless sensor node developed in the Laboratory. When the encapsulation for SHM is considered, the wireless sensors are easily connected with PZT and strain gauge. To monitor the different kinds of damage in the structure efficiently, the robust wireless sensor network protocol need to be researched.

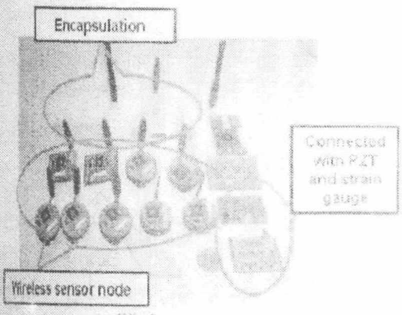

(a) Wireless sensors

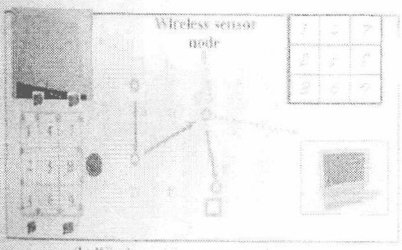

(b) Wireless sensor network

Figure 2. Health monitoring network using wireless sensors.

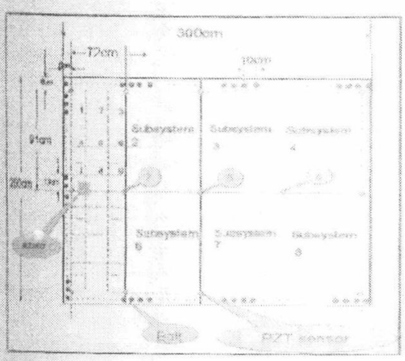

Figure 3. Multi-agent system for SHM

2.3 Multi-agent system

The multi-agent system (MAS) as shown in Fig. 3 was developed to coordinate the distributed, diverse, heterogeneous wireless sensor information for large structures [4]. Multi-agent system is viewed as a crucial technology not only for effectively exploiting the increasing availability of diverse, heterogeneous and distributed information sources, but also as a framework for building large, complex and robust distributed information processing systems which exploit the efficiencies of organized behavior. Multi-agent system based SHM system architecture is designed. A MAS based composite SHM system is studied as a case

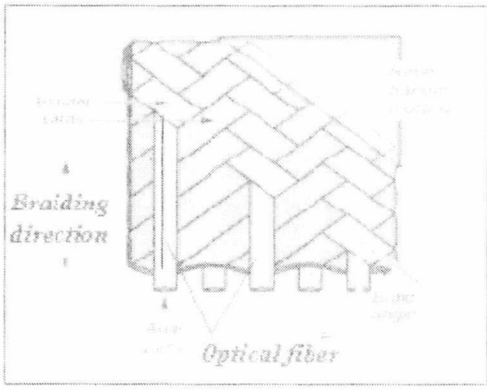

Figure 4. Braided composite with optical fiber

study to evaluate the efficiency of the proposed MAS based SHM system design and the advantages of the MAS based SHM system. Comparing to past system, many advantages can be obtained. The system can deal with geographically distributed networks, fuse different kinds of sensor data and give an efficient evaluation result of the large structure using uncomplicated logic; through collaboration, the structure damage can be identified automatically; useless data can be automatically discarded; using the agent learning ability, the sensor performance shifting and the influence from environment parameters can be eliminated.

2.4 Braided composite with optical fiber

3-D braided composite technology has stimulated a great deal of interest in the world at large [5]. Impacts from hail, debris, tools, etc. can delaminate conventionally-laminated composites because of the relatively weak resin interface between laminae. The through-the-thickness or interlacing reinforcement in braided composites has the potential to reduce or even eliminate delamination and thus reduce or eliminate strength degradation due to accidental damage. In addition, braided composites will potentially cost less than traditional laminated composites that are fabricated with unidirectional tape, because a 3-D, fully integrated structure can be directly fabricated into various structural shapes by adopting 3-D braiding technology, which does not require fiber cloth tailoring and layering. A reliable understanding of the properties of 3-D braided composites is of primary importance for the successful utilization of these materials.

A new method was proposed to study the mechanical performance of braided composite materials using embedded fiber optic sensors, as shown in Fig. 4. Experimental research is performed to devise the methods of incorporating the optical fiber into a 3-D braided composite structure. To validate the ability of the optic fiber to withstand the manufacturing process, the optical performance of the optic fiber is first studied before and after incorporation into the 3-D braided composites, and also after the entire manufacturing process of the 3-D braided composites. Also the method is used to monitor the molding process, such as Rein Transfer Molding (RTM) process. Using the braided fiber sensor, the mechanical performance of the material and mechanism of the damage failure were studied. Experiments were conducted to measure interval strain under loading condition of tension and bending in the 3-D carbon fiber braided composite specimens, both locally and globally. Experimental results show that multiple fiber optic sensors can be braided into the 3-D braided composites to determine its mechanical properties, providing a more accurate measurement method and leading to a better understanding of these materials.

3 MICROWAVE AND HOT-PRESS HYBRID SINTERING PROCESS

In order to improve the performance of PZT actuators, several processes including a hybrid sintering process and a hydrothermal process for synthesizing powders, were developed. The hybrid sintering process, which is the combination of 28 GHz microwave sintering and hot-press, was applied to the sintering of PZT actuators with the optimal sintering conditions [6, 7]. Due the rapid and uniform heating of the samples in microwave sintering process, the sintering time was reduced to about 1/8 of the time needed for the traditional technology. On the other hand, shorter sintering time results in less evaporation of Pb in the sintering process. The density of sintered samples was higher than 99% of the theoretical density due to high pressure of hot-press. The measurement results showed that the electromechanical coupling factor was increased significantly and the piezoelectric constants could be improved by nearly 40% with the hybrid process. In this chapter, the hybrid sintering and its application are introduced.

3.1 *Principle of microwave sintering process*

The hybrid sintering apparatus of microwave and hot-press used for the sintering of the PZT ceramics is schematically illustrated in Fig. 5. The applicator of the microwave sintering furnace is connected to the 28 GHz gyrotron, the power of which is 10 kW, capable of heating specimens up to 2000°C. The typical dimensions of the applicator are 600 mm in diameter and 900 mm in length, which allows a volume of 300 mm (diameter) by 300 mm (height) in the applicator to offer spatially uniform distribution of wave field.

On the other hand, the hot-press accessory is mounted in applicator of the microwave sintering furnace and the hydraulic press subsystem can deliver the maximum force of 49 kN. The die used in the hot-press accessory was made from alumina. Alumina lagging is also placed around the die to avoid heat dissipation. The preliminarily formed samples were covered with zirconia powders to prevent them from sticking to the alumina die.

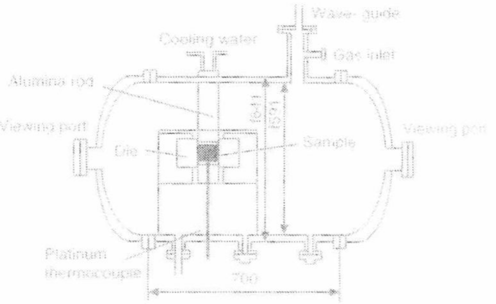

Figure 5. Schematic diagram of microwave and hot-press hybrid sintering apparatus.

3.2 *Preparation of sintering specimens*

The PZT specimens used in the study were made from PZT powder C82 developed by Fuji Ceramics Corporation. These powders was compacted into specimens of two different shapes with cold press under 200 MPa, one of which is a disk with the diameter of 17 mm and thickness of 15 mm and the other is a plate of 55 mm long, 35 mm wide and 20 mm thick. The binder of the specimens was burned out at 700°C for five hours. The specimens in disk shape were prepared for the measurement of piezoelectric properties and observation of microstructure, and those in plate shape were used for vibration test. The specimens were sintered with both the hybrid sintering process and the conventional sintering process for the comparison of performances.

In conventional sintering process, the surface temperature of the specimens is higher than internal temperature, since they are heated from the outside. However in the case of microwave sintering, the internal temperature is higher than surface temperature, since they are uniformly heated theoretically and the surface temperature becomes lower due to heat dissipation. In the hybrid sintering process, a number of specimens were stacked vertically and sintered together. The temperature of the specimens was measured with a platinum thermo- couple, the measurement error of which was less than 5°C. In order to measure the internal temperature, a hole of 5 mm in diameter and 1.5 mm in depth was made on the bottom specimen of the stack and the end of the thermo-couple was inserted into the hole. The measured temperature was used in the feedback control of the output power

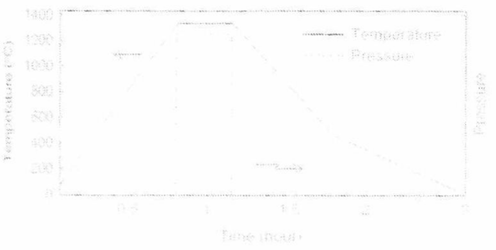

Figure 6 Temperature and pressure schedules of hybrid sintering process.

of the microwave generator to ensure the temperature of the specimens in agreement with the scheduled temperature of the sintering process.

The temperature scheduling of microwave sintering process and the pressure scheduling of hot-press are shown in Fig. 6. In the hybrid sintering process, the temperature of specimens was raised from the room temperature to the sintering temperature at the rate of 6000 °C/hour, maintained for 30 minutes and then cooled at the same rate as that of the heating phase. The whole cycle of the hybrid sintering process should have taken about two hours. However, the temperature of specimens decreases much more slowly than the scheduled rate due to the lack of forced cooling and the actual sintering process took about ~ hours. Sintering temperatures between 1100 °C and 1250 °C were tried at the step of 50 °C in the experiment. The pressure of hot-press was raised to the predetermined value (20 MPa or 40 MPa) when the temperature of the PZT specimens was maintained at the maximum sintering temperature.

3.3 *Evaluation of properties*

The surfaces of the specimens sintered with the hybrid sintering process were polished in a polishing machine and the thickness was reduced to 1 mm from the original thickness of 1.5 mm. The density and porosity of the specimens were measured with the Archimedes technique using water. The phase structure of the specimens was established by X-ray diffraction (XRD) using CuKα. Furthermore the sintered specimens were mirror-polished and chemically etched in 30% HNO_3 solution added with several drops of HF. The microstructure of etched surface of the specimens was observed under scanning electron microscope (SEM), and the grain size was measured with linear intercept method.

The specimens for the measurement of k_p were disks of 15 mm in diameter and 1 mm in thickness, while the specimens for the measurement of k_{31} were plates of 12 mm long and 3 mm wide cut from the disks. After sputtered with gold electrodes on both surfaces, specimens were polarized in a silicon oil bath with a DC filed of 2 kV/mm and oil temperature of 170 °C for 30 minutes, and then cooled down to 50 °C in the field. The dielectric constants of the polarized specimens were measured at the frequency of 1 kHz. The electromechanical coupling factors k_p and k_{31} and the frequency constant N_p were determined by the resonant-antiresonant frequency method with a HP4194A impedance analyzer. The elastic compliance coefficient S_{11}^E, piezoelectric constant d_{31} and the frequency constant N_p are calculated from the following formulas:

$$k_{31} = \frac{d_{31}}{\sqrt{\varepsilon_{33} \cdot S_{11}}} \qquad f_r = \frac{1}{2l} \cdot \frac{1}{\sqrt{\rho \cdot S_{11}}}$$

$$N_p = f_r \cdot d \qquad \varepsilon = \frac{\varepsilon_{33}}{\varepsilon_0}$$

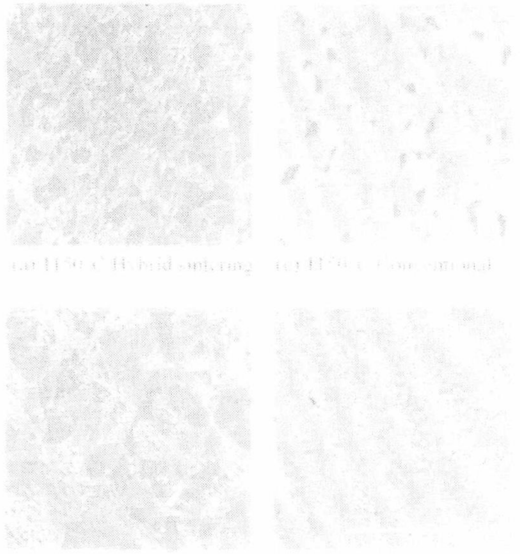

(a) 1150 °C Hybrid sintering (c) 1150 °C Conventional

(b) 1250 °C Hybrid sintering (d) 1250 °C Conventional

Figure 7 The SEM photographs of microstructure of hybrid and conventional sintered specimens.

where f_r is the resonance frequency, l is length of specimens, d is diameter of specimens, and ε_0 is dielectric constant in a vacuum.

The same measurements were also performed for specimens of the same shape fabricated with conventional sintering process. The measurement results are used in the comparison to show the improvement of performances due to the new sintering process.

The dependence of the grain size of the specimens on the sintering temperature was also investigated. The SEM microstructures are shown in Fig. 7 (a) and (b) for specimens of the hybrid sintering process and in Fig. 7 (c) and (d) for specimens of the conventional sintering process. It can obviously seen that the average

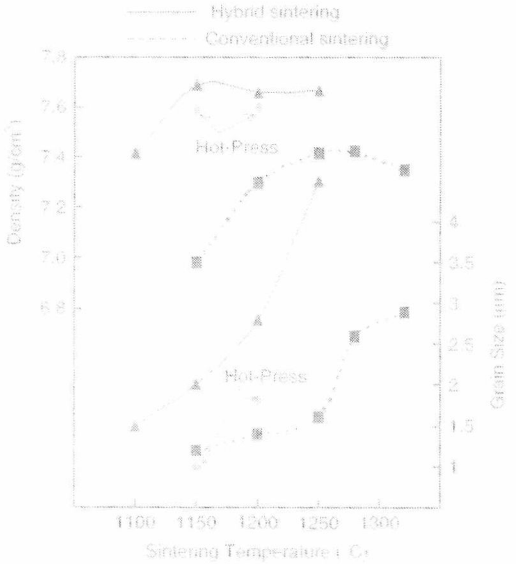

Figure 8 Density and grain size

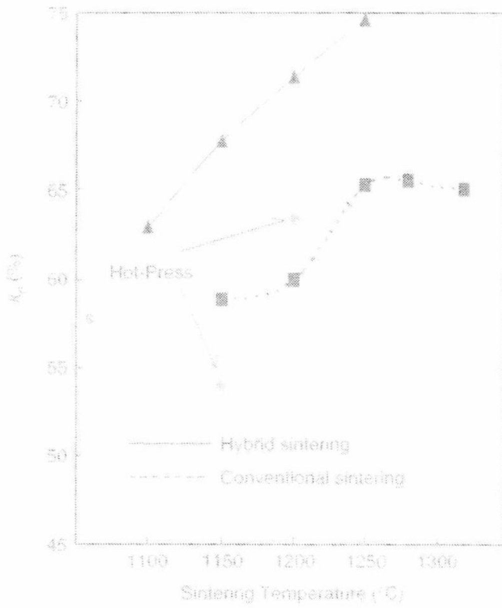

Figure 9 Electromechanical coupling factor

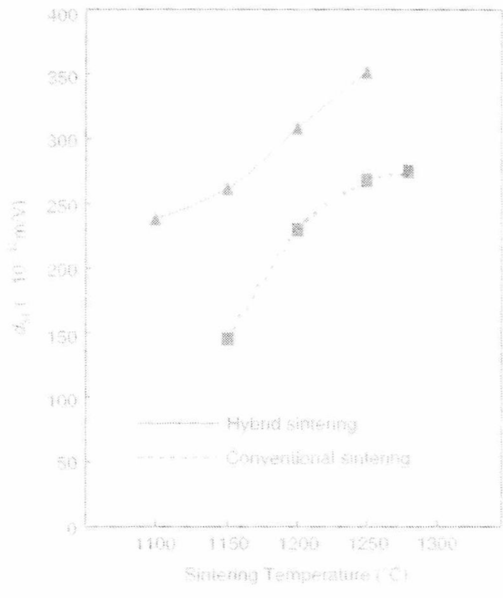

Figure 10 Piezoelectric constants

grain size of specimens of the hybrid sintering process, which is about 4 μm for the sintering temperature of 1250°C, is larger that that of the specimens of conventional sintering process. It can also be seen from Fig. 7 (a) and (b) that the average grain size increases with the sintering temperature. For the conventional sintering process, only porous specimens can be obtained at 1150°C as shown in Fig. 7 (c), but pores were significantly reduced when sintered at 1250°C, as shown Fig. 7 (d). For the hybrid sintering process, specimens with few pores can be obtained even at 1150°C as shown in Fig. 7 (a).

Fig. 8 illustrates the dependence of the density and grain size of the specimens on the sintering temperature of the hybrid sintering process and the conventional process. The theoretical density of the material is 7.75 g/cm³. The density of the specimens fabricated with hybrid sintering process was larger than that of conventionally sintered specimens when the sintering temperature was above 1100°C. For the conventionally sintered specimens, the density increases with sintering temperature below 1250°C but decreases slightly over 1250°C while the grain size increases with sintering temperature in the whole considered temperature range. For the specimens of hybrid sintering process, no strong correlation was observed between the density and grain size.

Figs. 9 and 10 show the electromechanical coupling factor k_p and the piezoelectric constant d_{31} as functions of the sintering temperature. The d_{31} and k_p of the specimens of the same sintering process exhibit very similar tendency of variation. Moreover, The d_{31} and k_p of the hybrid-sintered specimens are much larger than those of the conventionally sintered specimens. The maximum value of k_p of hybrid-sintered specimen, achieved at the sintering temperature of 1250°C, is approximately 75%, and the maximum value of d_{31}

of the same specimen, achieved at the same sintering temperature, is about 360×10^{-12} m/V, nearly 40% larger than 260×10^{-12} m/V, the d_{33} of conventionally fabricated specimens. If the curves of d_{33} and k_p are compared with those of grain size in Figure 2-4, it can be concluded that the increase of both d_{33} and k_p is attributed to the increase of grain size in the specimens. In the conventional sintering, the percentage of pore usually increases with increasing grain size so that the piezoelectric constant d_{33} and coupling factor k_p decrease. However, the grain size was increased without increasing pores in hybrid sintering process due to the rapid and internal heating.

4 FUNCTIONALLY GRADED PIEZOELECTRIC ACTUATORS

The conventional bimorph actuators are manufactured by bonding two piezoelectric elements to a metal shim layer. Due to discontinuity of material properties, stress concentration, which is the cause of delamination and cracks, is generated at the interfaces between the PZT layers and the shim layer. In order to improve the reliability of PZT bending actuators, a new type of functionally graded (FG) PZT bending actuator was designed and fabricated. The material compositions with different dielectric and piezoelectric constants were selected from the PNN-PZ-PT ($Pb(Nb_{2/3}Ni_{1/3})O_3 - PbZrO_3 - PbTiO_3$) family and used as the four layers in the new FG PZT actuator [8,9,10]. The piezoelectric constant and dielectric constant were graded oppositely in the thickness direction. Stress distribution of the FG PZT actuator under external voltage was analyzed using FEM and the simulation results showed the stress discontinuity in the new actuator is smaller than that of traditional bimorph actuator. Durability test was performed with the fabricated FG PZT actuators and conventional bimorph actuator and the results showed that the durability of the FG PZT actuators is much higher than that of bimorph actuator.

4.1 *Material compositions and thickness of layers*

The authors proposed a new type of functionally graded piezoelectric actuator and illustrated that the stress discontinuity could be significantly reduced in the FG piezoelectric actuator using FEM analysis in the former study. As the task of this research project, the FG piezoelectric actuator was designed and fabricated.

To obtain large bending deflection, the combination of a high-performance piezoelectric material with large piezoelectric constants but small dielectric constant (material-H) and a low-performance piezoelectric material with small piezoelectric constants

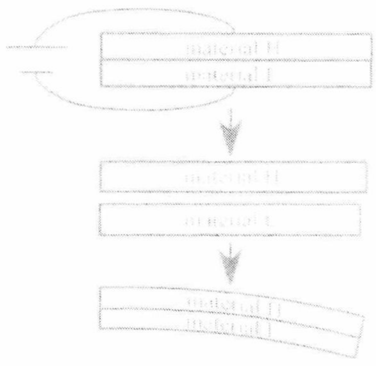

Figure 11. Mechanism of bending deflection.

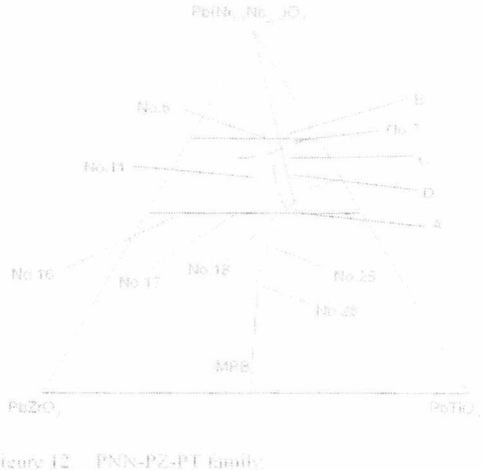

Figure 12. PNN-PZ-PT family.

but large dielectric constant (material-L) is required. The large dielectric constant can reduce the voltage loss in the low-performance piezoelectric material. As shown in Fig. 11, bending deformation is generated in the actuator with the same mechanism as that of unimorph actuator when a voltage is applied to a two-layer actuator of the two materials. However, large stress discontinuity is also induced in the interface of the two materials. In order to increase the generated deformation, the difference of the material properties of the two layers should be as large as possible. On the other hand, the larger the difference of material properties is, the larger the stress discontinuity is. In order to reduce the stress discontinuity the material properties should be graded smoothly in the thickness direction. But smooth distribution of material properties raises difficulties in the practical fabrication. Hence, a four-layer structure was used in the FG actuator. The material compositions of the four layers were chosen from the PNN-PZ-PT family.

Table 1. Material compositions.

A	$Pb(Ni_{1/3}Nb_{2/3})_{[illegible]}(Ti_{[illegible]}Zr_{[illegible]})_{[illegible]}O_3$
B	$Pb(Ni_{1/3}Nb_{2/3})_{[illegible]}(Ti_{[illegible]}Zr_{[illegible]})_{[illegible]}O_3$
C	$Pb(Ni_{1/3}Nb_{2/3})_{[illegible]}(Ti_{[illegible]}Zr_{[illegible]})_{[illegible]}O_3$
D	$Pb(Ni_{1/3}Nb_{2/3})_{[illegible]}(Ti_{[illegible]}Zr_{[illegible]})_{[illegible]}O_3$

Table 2. Material properties.

	d_{31} (10^{-12} m/V)	s_{11}^E (10^{-12} m²/N)	k_p (%)	$\varepsilon/\varepsilon_0$
A	−311	16.03	62	6496
B	−61	8.67	0	20971
C	−232	9.78	0	16469
D	−331	14.11	41	11288

The piezoelectric constants, dielectric constant and coupling factor of 40 compositions in PNN-PZ-PT family shown in Fig. 12 were measured, and four of them were chosen as the materials of the four layers in the FG actuator. The compositions of the four materials are shown in Table 1 and their properties are shown in Table 2. Material A has the largest d_{31} but smallest ε while material B has the smallest d_{31} but largest ε. The four materials were laminated in the order of A-D-C-B.

4.2 *Measurement of performance*

Since the internal stress distribution is very difficult to measure, durability was used to evaluate the performance of the actuators. Empirically, improvement of stress distribution and mechanical strength at the interface of layers will suppress the fatigue of the actuator and consequently improve the durability of the actuator. In the durability test, the vibration of a cantilever actuator was excited by a voltage at various frequencies. The size of the FG bending actuators is 42 × 8 × 0.9 mm. As shown in Fig. 13, the displacement of vibration at the free end was measured with a laser displacement sensor (KEYENCE, LC-2440) and the temperature of the actuator was measured near the clamped end by a thermo-couple. The variation of amplitude and temperature with time was recorded by a data acquisition system based on LabView. In order to investigate the influence of vibration amplitude, the test was performed at various frequencies.

4.3 *Frequency characteristics and damping ratio*

A random signal (white noise) was applied to the actuators for the measure of the frequency response of the FG actuator and the bimorph actuator. The results are shown Fig. 14. The peak-to-peak value of voltage applied to the FG actuator is 100 volts and that applied to the bimorph actuator is 50 volts. From the frequency response, the natural frequencies of the FG actuator and bimorph actuators were estimated to be 360 Hz and 335 Hz, respectively. It can further be seen that the structural damping factor of the bimorph actuator is much higher than that of the FG actuator. In order to estimate the damping ratio of the actuators, their free vibration responses were measured and the results are shown in Fig. 15. The estimated damping ratio of the FG actuator is 0.016 while that of the bimorph actuator is 0.086 for the first mode. The high damping ratio of bimorph actuator can be attributed to the material damping of bonding layers as discussed in the later section.

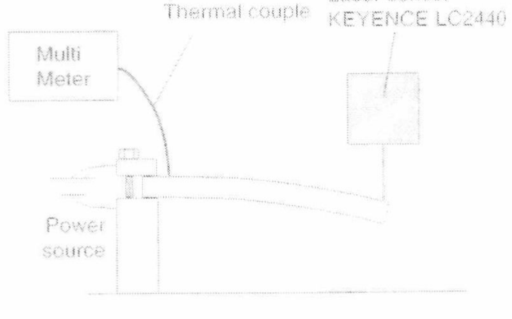

Figure 13. Experimental setup for durability test.

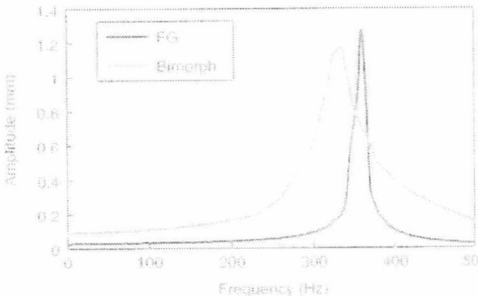

Figure 14. Frequency response (Applied signal: white noise; Voltage: 50V p-p for bi-morph and 100V p-p for FGM).

4.4 *Durability at low frequency*

The FG piezoelectric actuators and bimorph actuator were driven at 20 Hz and 100 Hz, much lower than the resonance frequency. In order to generate bending vibrations of the same amplitude in the actuators, the voltages applied to the FG actuator and the bimorph actuator are set to 500 volts and 80 volts (peak-to-peak), respectively. Figure 16 shows the results of durability test at 20 Hz. There is neither obvious temperature rise, nor amplitude drop during the test period

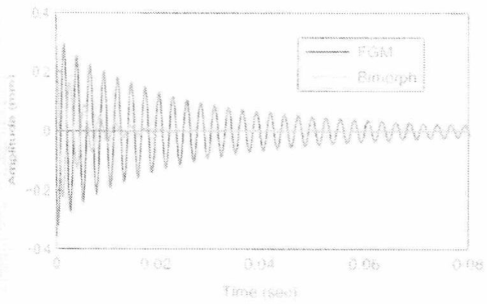

Figure 15. Free vibration of the two actuators.

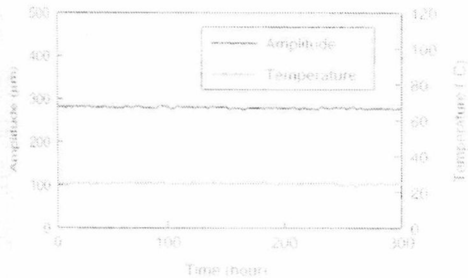

(a) Amplitude and temperature of FG actuator

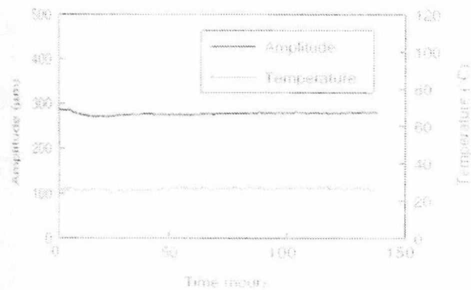

(b) Amplitude and temperature of bimorph actuator

Figure 16. Results of durability test at 20 Hz.

at this frequency. The bimorph actuator broke down due to cracks in 138 hours (about 10^{7} cycles), while the FG actuators did not break down after 300 hours (2.16×10^{7} cycles) of test. The average lifetime of the three bimorph actuators tested was 146 hours, while the lifetime of all the three FG actuators was longer than 300 hours. The amplitude of vibration of both the FG actuators and the bimorph actuators was about 280 μm, a little smaller than the simulation result of about 350 μm. The experimental results also showed that much higher voltage is required for FG actuator to generate the same amount of displacement as conventional bimorph actuators. One of the reasons is that the effective thickness of the FG actuator is much larger than that of the bimorph actuator.

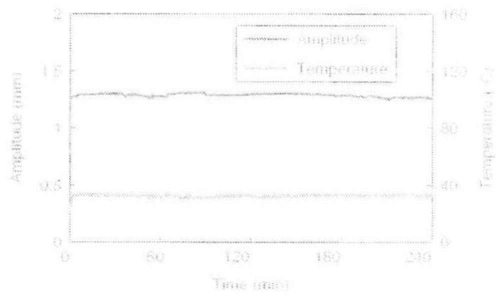

(a) Amplitude and temperature of FG actuator

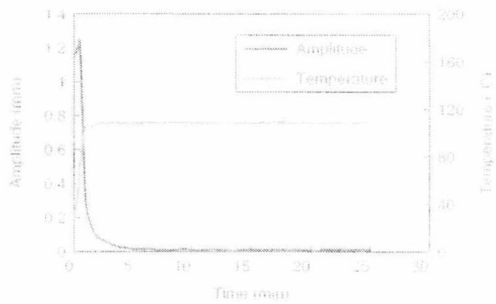

(b) Amplitude and temperature of bimorph actuator

Figure 17. Results of durability test at resonance

4.5 *Durability at resonant frequency*

Durability test was also performed at the respective resonant frequencies of the FG actuators and the bimorph actuators. The peak-to-peak amplitude of the voltage applied to the FG actuator was set to 40 volts while that applied to bimorph actuator was set to 14 volts. The variation of vibration amplitude and actuator temperature was shown in Fig. 17. In spite of lower voltage, the amplitude of vibration is larger than that of former section due to resonance. The amplitude of FG actuator remained constant during the test period of 240 minutes (about 5×10^{6} cycles) and the temperature rise was less than 10°C. However, the temperature of bimorph actuators rose to about 110°C and the amplitude almost dropped to 0 in less than 2 minutes. Even though the amplitude remained at very lower level thereafter, the temperature remained at 110°C. The bimorph actuator broke down due to delamination in 25 minutes (about 5×10^{5} cycles) after the start of test. Two bimorph actuators and two FG actuators were tested. The average lifetime of the two tested bimorph actuators was 24 minutes, but both the FG actuators did not fail in the test period of 240 minutes.

The decrease of vibration amplitude of the bimorph actuators may be attributed to the depolarization of piezoelectric material and the change of vibration characteristics of the actuators. The Curie temperature of the piezoelectric material used in the bimorph